J Mater Sci (2019) 54:4917–4927

Energy materials

From biological waste to honeycomb-like porous carbon for high energy density supercapacitor

Yahui Wang[1], Ziyu Zhao[1], Weiwei Song[1], Zhichao Wang[1], and Xiaoliang Wu[1,*]

[1] *Department of Chemistry, College of Science, Northeast Forestry University, 26 Hexing Road, Harbin 150040, People's Republic of China*

Received: 22 August 2018
Accepted: 30 November 2018
Published online: 6 December 2018

ABSTRACT

We develop a facile and sustainable method for the synthesis of three-dimensional (3D) interconnected honeycomb-like porous carbon (HPC) derived from sunflowers stem. The optimized sample has large specific surface area with 3D interconnected honeycomb-like porous structure and high oxygen content. Due to their synergistic effect, the HPC-2 material shows a high specific capacitance of 349 F g^{-1} at 1 A g^{-1}, good rate capability (247 F g^{-1} at 50 A g^{-1}) and excellent cycling stability (retaining 98.6% after 10000 cycles) in 6 M KOH aqueous electrolyte. Moreover, the HPC-2//HPC-2/MnO_2 asymmetric supercapacitor shows a high energy density of 58.8 W h kg^{-1} and good electrochemical stability (83.1% of initial capacitance retention after 10000 cycles). Therefore, these unique properties enable the material to become a promising high-performance electrode material for supercapacitors.

Introduction

Among different energy storage equipments, supercapacitors have attracted tremendous attentions owing to their unique characteristics, such as rapid charge/discharge rates, ultrahigh power density and excellent electrochemical stabilization [1–4]. However, the supercapacitors usually suffer from low energy density (less than 10 W h kg^{-1}) compared with batteries, which limits their practical applications [5–7]. To meet the fast-growing energy needs for next generation supercapacitors, there is a critical need to improve the energy density without sacrificing large power density. In accordance with the energy density formula, $E = 0.5\ CV^2$, C is the gross capacity of the supercapacitor and V is the potential range. Hence, an increase in energy density can be achieved through increasing the specific capacity or/and potential range. Recently, an effective method to increase the energy density is to construct asymmetric supercapacitors. The combination of different voltage ranges of the positive/negative electrodes provides an optimized operation voltage in the asymmetric supercapacitors, resulting in greatly enhanced energy density, such as $Ni(OH)_2$/graphene//porous graphene [8], sandwiched graphene/porous carbon//LDH [9], MnO_2//Fe_2O_3 [10].

Address correspondence to E-mail: wuxiaoliang90@163.com

https://doi.org/10.1007/s10853-018-03215-8

Among different electrode materials, carbon materials have the advantages of large specific surface area, moderate cost, good chemical inertness and good electrical conductivity, which make them as common electrode materials for supercapacitor [11–14]. Activated carbon materials (ACs) have been used as the first candidate electrode material for commercial supercapacitor. However, activated carbon usually suffers from long diffusion distance and large internal resistance, which seriously affect the specific capacitance and rate performance of supercapacitor [7].

Recently, biomass-based carbon materials have attracted tremendous interest with an excellent performance as electrode material in supercapacitors and battery because of the massive source, renewable raw materials, moderate cost and unique porous structure of biomass precursors [15–20]. For example, Xu reported a facile way to synthetize three-dimensional (3D) flexible carbonaceous gels using watermelon as the carbon source followed incorporated Fe_3O_4 nanoparticles into the networks of the carbonaceous gels, and the obtained sample shows high specific capacitance and excellent electrochemical stabilization [21]. Lei synthesized nitrogen-doped porous carbon using potato waste residue as the carbon source, zinc chloride as the activating agent and melamine as nitrogen source. The obtained material shows high specific capacitance [22].

As one of the fastest growing oil crops in the world, the annual output of sunflower is about 25 million tons, resulting in a large amount of biological waste in urgent need of treatment. Hence, a facile and sustainable method was developed for the synthesis of three-dimensional (3D) interconnected honeycomb-like porous carbon (HPC) derived from sunflowers stem. The optimized sample has large specific surface area with 3D interconnected honeycomb-like porous structure and high oxygen content. Due to their synergistic effect, the HPC-2 material shows a high specific capacity of 349 F g^{-1} at 1 A g^{-1}, outstanding rate performance (247 F g^{-1} at 50 A g^{-1}) and excellent cycling stability (retaining 98.6% after 10000 cycles) in 6 M KOH aqueous electrolyte. Moreover, the HPC-2//HPC-2/MnO_2 asymmetric device shows a high energy density of 58.8 W h kg^{-1} and good electrochemical stabilization (83.1% of initial capacity retention after 10000 cycles).

Experimental sections

Materials

Sunflower stems are produced in Heilongjiang province, China. KOH, $KMnO_4$ and hydrochloric acid were acquired from Tianjin Yongda Chemical Reagent Co., Ltd. All chemicals and reagents are of analytical grade and were used without any further treatment.

Synthesis of honeycomb-like porous carbon (HPC)

Sunflower stem powders can be well dispersed in distilled water to form a suspension under vigorous stirring. Two grams of sunflowers stem powders and different masses of KOH (1, 2, 3 g) were firstly mixed in 150 mL stilled water. After evaporation of the stilled water at 95 °C under vigorous agitation, the obtained mixture was carbonized under N_2 flow at 700 °C for 2 h. Then, the obtained material was washed with dilute HCl solution, distilled water and dried at in a vacuum oven. The obtained products were denoted by HPC-x, where x refers to the mass ratios of KOH.

Synthesis of HPC-2/MnO_2 composite

Eighty milligrams of HPC-2 samples was dispersed into (1.08 mmol, 100 mL) potassium hypermanganate solution and stirred for 120 min. Then, the mixture was heated by a household microwave oven (Galanz, P70F20L-DG, 700 W) for 10 min. Finally, the product was filtered, washed several times with distilled water, and dried in a vacuum oven.

Characterization methods

The microstructures of the materials were checked by a scanning electron microscopy (Hitachi S-4800) and transmission electron microscopy. X-ray diffraction (XRD) patterns were recorded on a powder XRD system (TTR-III) equipped with Cu Kα radiation (λ = 0.15406 nm). X-ray photoelectron spectroscopy (XPS) was performed by a PHI5700ESCA spectrometer with Al Kα radiation (1486.6 eV); Raman spectra were checked by a JY HR-800 Raman spectrometer (JobinYvon, France). N_2 adsorption/desorption tests were investigated by N_2 adsorption at 77 K on an

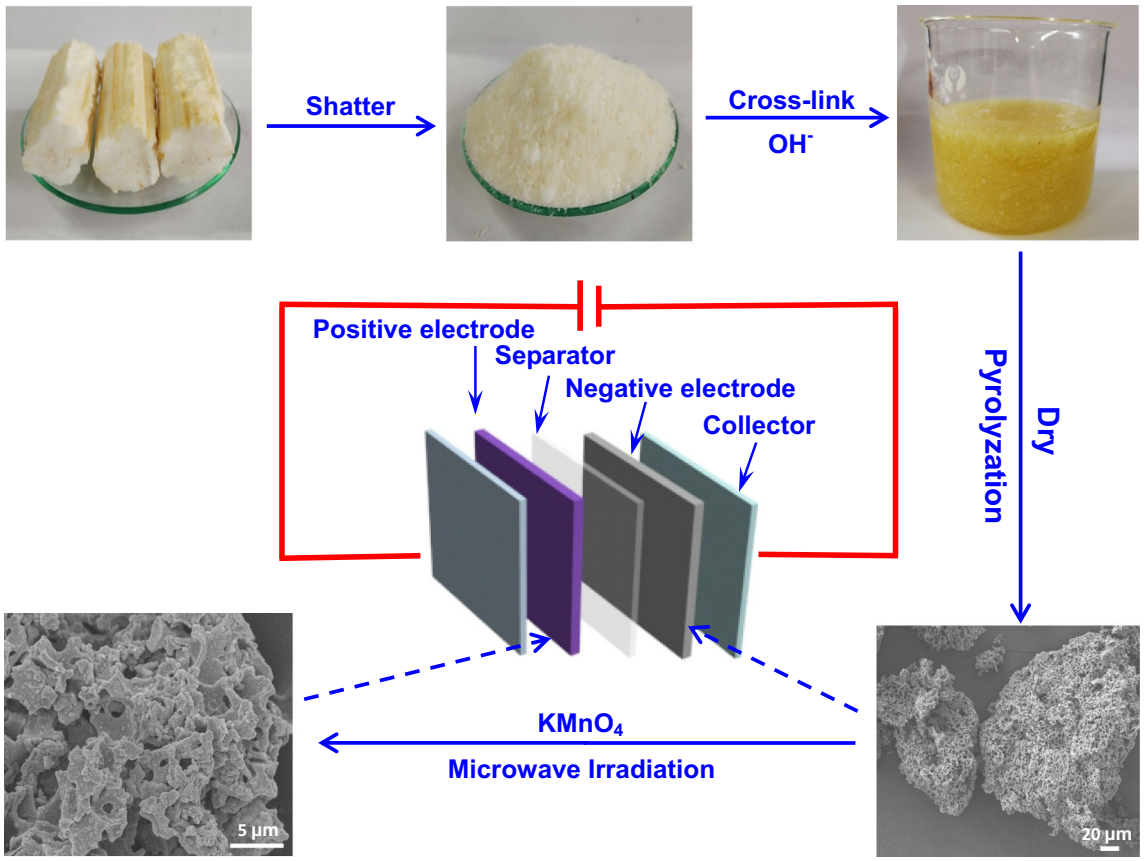

Figure 1 Schematic illustration of the preparation processes of the asymmetric supercapacitor.

ASAP 2020 (Micromeritics, USA). The specific surface area was calculated by the modified Brunauer–Emmett–Teller (BET) method, and the pore size distributions of the samples were obtained by density functional theory (DFT) model.

Electrochemical measurements

The electroactive materials, carbon black, tetrafluoroethylene were mixed in ethanol at 75:20:5 by mass ratio to obtain slurry. The slurry was pasted onto the Ni foam (1 cm × 1 cm) and dried in oven. Ni foam coated with electroactive materials was used as the working electrode; platinum foil and Hg/HgO electrode were used as the counter and reference electrodes, respectively. All the electrochemical tests were recorded by a CHI 660E electrochemical workstation at room temperature.

Asymmetric supercapacitor was assembled using a glassy fibrous as separator and tested with a two-electrode cell in 1.0 M Na_2SO_4 aqueous electrolyte. The loading mass ratio of positive electrode and positive electrode was estimated by the following formula:

$$\frac{m_+}{m_-} = \frac{C_- \times V_-}{C_+ \times V_+} \tag{1}$$

which C is the specific capacity (F g^{-1}), V is the voltage range (V), and m is the mass of the electrode material (g).The specific capacity (C) was calculated by the following formula:

$$C = \frac{I\Delta t}{m\Delta V} \tag{2}$$

$$C = \frac{\int I dV}{vmV} \tag{3}$$

Which I is the current density, ΔV is the discharge time Δt, V is potential, v is the potential scan rate, and m is the mass of the electroactive materials.The power density (P) of the supercapacitors was calculated using equation:

$$P = \frac{E}{t} \tag{4}$$

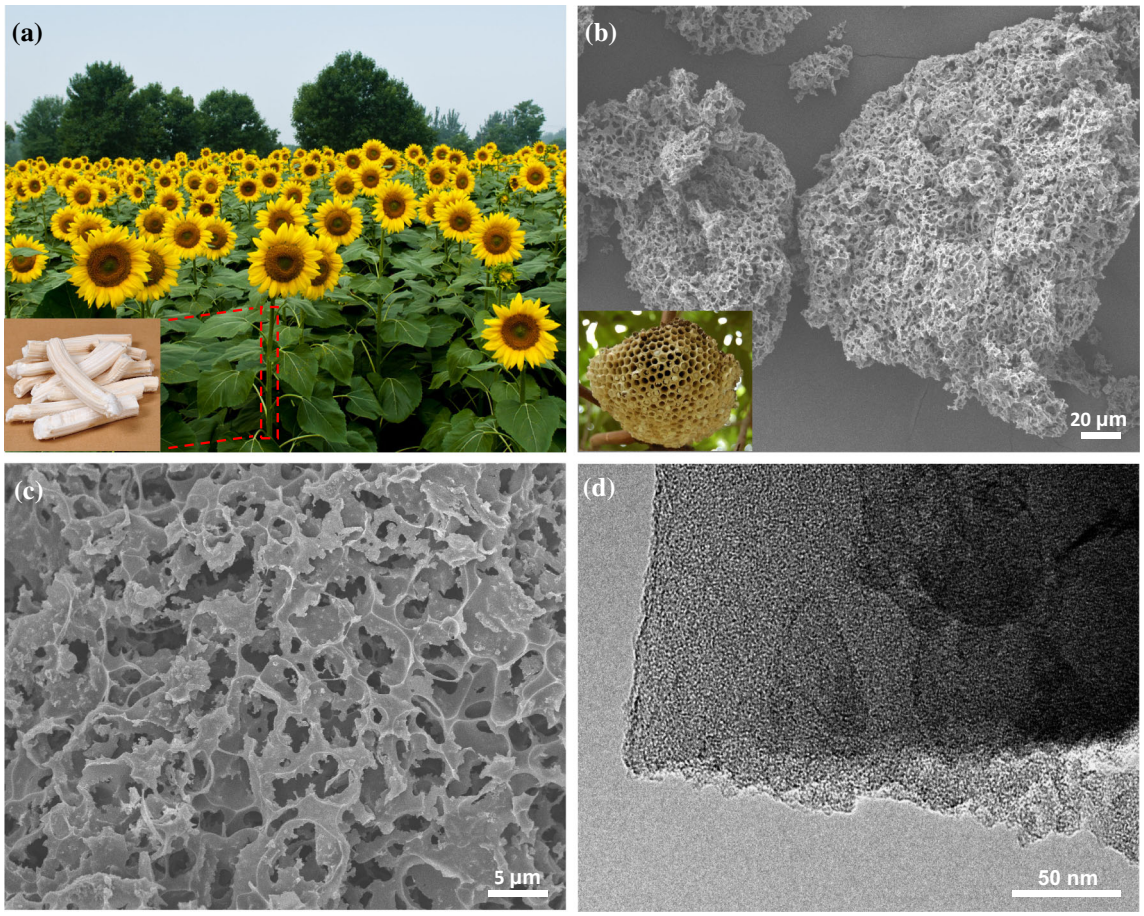

Figure 2 **a** The photograph of sunflowers. Inset of (**a**) is the photograph of sunflowers stem. **b** SEM image of HPC-2. Inset of (**b**) is the photograph of a honeycomb. **c** SEM image of HPC-2. **d** TEM image of HPC-2.

Which t is the discharge time (s) and E is energy density (W h kg^{-1}).

Results and discussion

Alkali catalysis can promote the pyrolytic decomposition of the sunflowers stem precursor, resulting in cross-linked foam structure by the interactions between the base and biopolymer in the precursor (Fig. 1). After pyrolysis, a 3D interconnected honeycomb porous structure is formed. Scanning electron microscopy (SEM) image of the HPC-2 sample (Fig. 2b) exhibits 3D honeycomb-like porous structure, which is in favor of the fast ion diffusion and electron transfer during charge–discharge process [13]. High-resolution SEM image of the HPC-2 sample (Fig. 2c) confirms its 3D highly interconnected porous framework with the pore sizes ranging from 1 to 3 μm. The corresponding element mapping images demonstrate the uniform distribution of C (Fig. S1b) and O (Fig. S1c). In addition, transmission electron microscopy (TEM) image of the HPC-2 sample exhibits massive micropores on the surface of carbon wall (Fig. 2d), which is in favor of the energy storage for supercapacitors. Furthermore, the HPC-1 and HPC-3 samples have the similar 3D honeycomb-like porous structure with HPC-2. With increasing ratio of KOH to sunflower stem powders, the thickness of carbon wall for HPC becomes thinner until fragmentation.

The structure characteristics of the as-prepared materials were further investigated by XRD and Raman. All XRD patterns (Fig. 3a) exhibit two characteristic peaks at around 24° and 44°, corresponding to the (002) and (100) plane reflection of carbon material. Compared with HPC-1 and HPC-3, HPC-2 shows two more broader and weaker diffraction peaks, meaning that the HPC-2 samples have more defect and disordered structure [23]. From the Raman analysis results (Fig. 3b), two peaks located at around

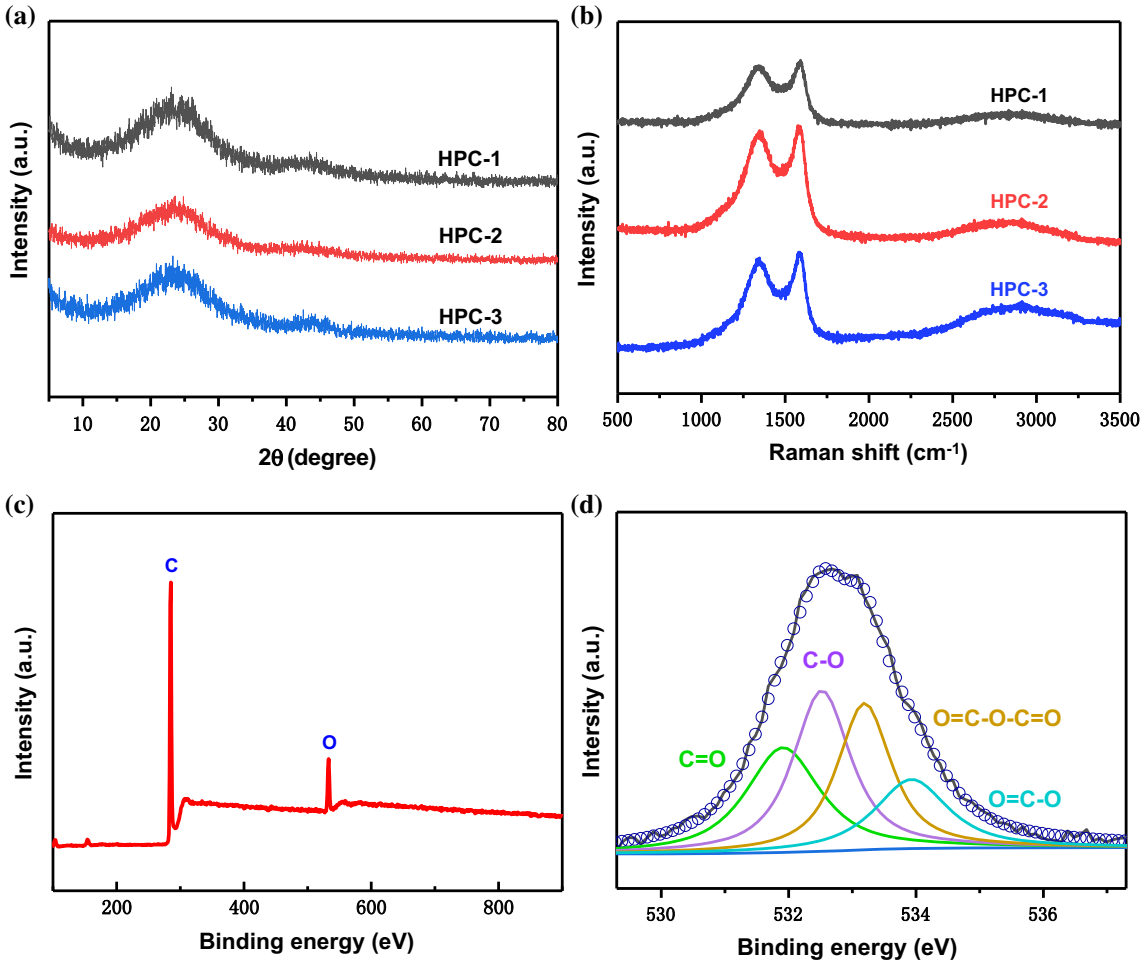

Figure 3 **a** XRD patterns of the HPC-1, HPC-2 and HPC-3 samples. **b** Raman spectra of the HPC-1, HPC-2 and HPC-3 samples. **c** XPS spectra survey of HPC-2 sample. **d** High-resolution O 1*s* spectra of the HPC-2 sample.

1340 cm^{-1} and 1590 cm^{-1} are attributed to the D peak (defects and disorder carbon) and G peak (graphitic carbon) of carbon material, respectively [24, 25]. The I_D/I_G ratio of HPC-2 was 0.96, higher than HPC-1 (0.93) and HPC-3 (0.94), further confirming that HPC-2 has more defects and disordered structure.

The surface chemical state of the HPC-2 material was determined by X-ray photoelectron spectroscopy (XPS). As shown in Fig. 3c, elemental analysis by XPS reveals that C and O contents are 90.54 at.% and 9.46 at.%, respectively. The high-resolution O1*s* spectra were further carried out to analyze their surface chemical states. As shown in Fig. 3d, The high-resolution O1*s* spectra for HPC-2 sample was deconvoluted into four peaks as follows: C=O (531.9 eV), C–O (532.5 eV), O=C–O–C=O (533.2 eV) and O=C–O (534.0 eV) [26]. It is worth noting that oxygen functional groups can not only offer some pseudocapacitance, but also improve surface hydrophilicity [25].

The porous textures of the as-obtained materials were analyzed by N_2 adsorption/desorption isotherms. All the samples show the combined features of type-I and-IV isotherms, suggesting the existence of micropores. The surface area of the HPC samples first increases with pyrolysis temperature, going from 1318 $m^2\ g^{-1}$ for HPC-1 to 1657 $m^2\ g^{-1}$ for HPC-2, and then decreases to 1490 $m^2\ g^{-1}$ for HPC-3. The pore size distributions were calculated by density functional theory model. As shown in Fig. 4b, pore size distribution of all the samples has mainly concentrated between 0.5 and 2 nm, further confirming the existence of massive micropores.

Electrochemical measurements were first performed by cyclic voltammogram (CV) using a three-

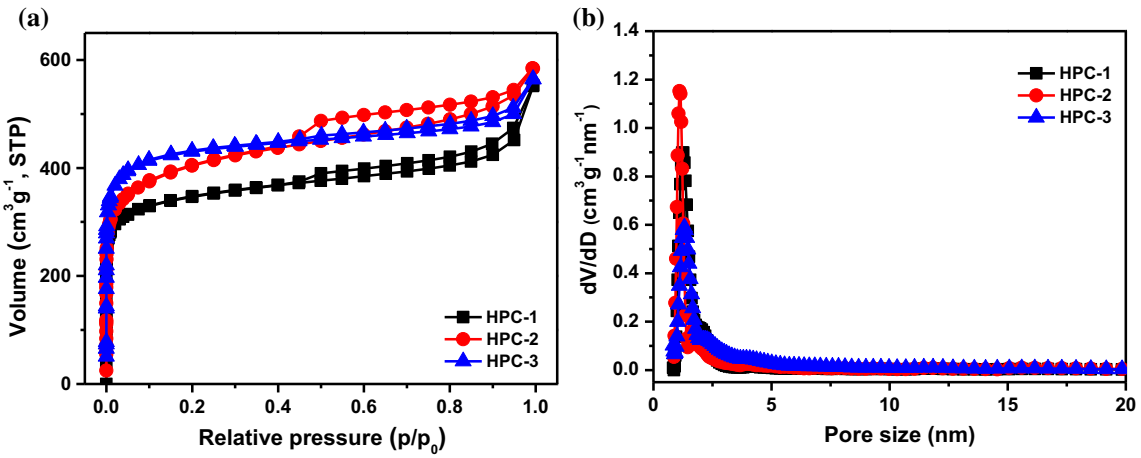

Figure 4 **a** Nitrogen adsorption–desorption isotherms of HPC-1, HPC-2 and HPC-3 samples. **b** Pore size distribution of HPC-1, HPC-2 and HPC-3 samples.

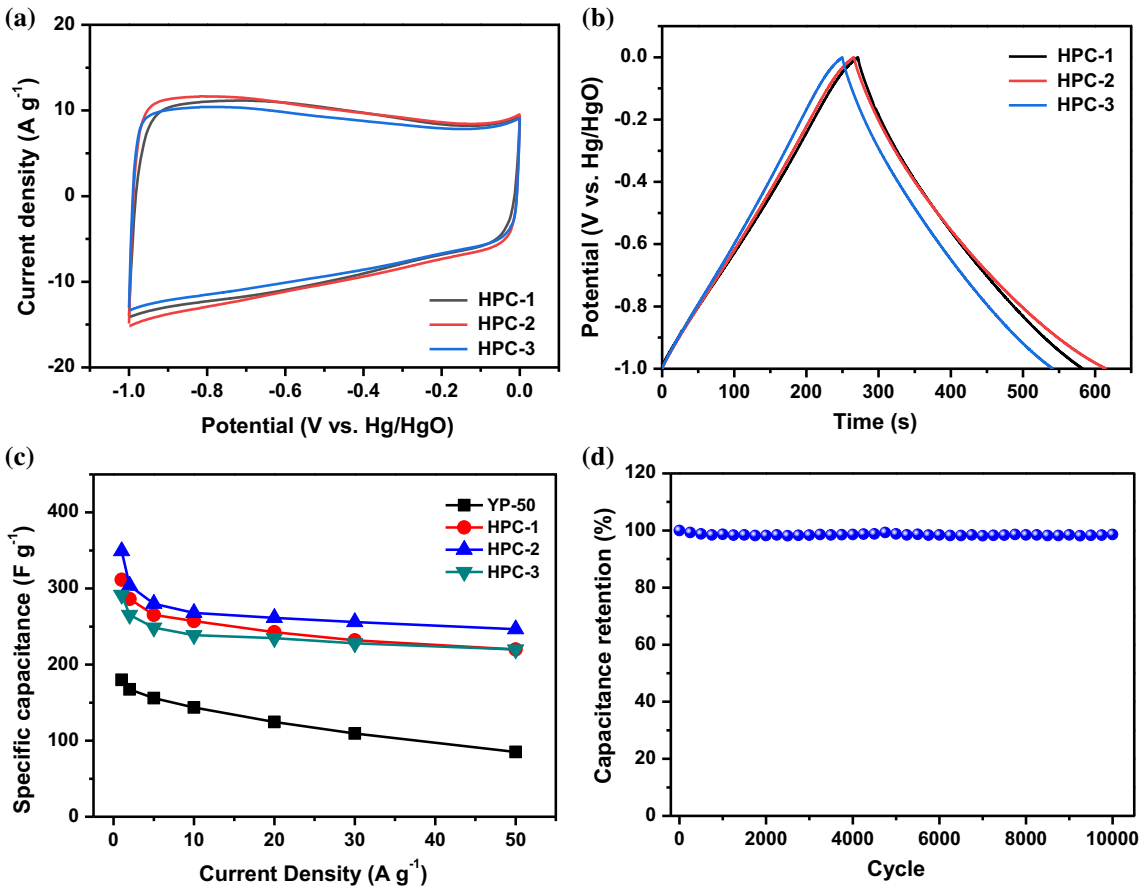

Figure 5 **a** CV curves of the HPC-1, HPC-2 and HPC-3 electrodes at a scan rate of 50 mV s^{-1}. **b** Galvanostatic charge/discharge curves of the HPC-1, HPC-2 and HPC-3 electrodes at a current densities of 1 A g^{-1}. **c** Specific capacitances of the YP-50, HPC-1, HPC-2 and HPC-3 electrodes at different current densities. **d** Cycling stability of the HPC-2 electrode at 200 mV s^{-1} for 10000 cycles.

electrode system in 6 M KOH solution to evaluate the supercapacitor performance of the HPC samples. Figure 5a shows the CV profiles of the HPC materials at a scan rate of 50 mV s^{-1}. All the samples show

Table 1 Summary of electrochemical performance for biomass-based carbon electrode materials

Material	Activation method	Specific surface area ($cm^2\ g^{-1}$)	C ($F\ g^{-1}$)	Electrolyte	References
Auricularia	$ZnCl_2$	1607	347 (1.0 A g^{-1})	6 M KOH	[7]
Sugar cane	$CaCl_2$	945.76	323 (1.0 A g^{-1})	6 M KOH	[17]
Lignin	KOH	907	165 (0.05 A g^{-1})	1 M H_2SO_4	[27]
Chicken eggshell	KOH	1575	297 (1.0 A g^{-1})	1 M KOH	[28]
Coconut shell	$ZnCl_2$	1874	248 (0.5 A g^{-1})	6 M KOH	[29]
Rice husk	H_3PO_4	1493	112 (1.0 A g^{-1})	1 M Na_2SO_4	[30]
Algae	KOH	905.9	287.7 (0.2 A g^{-1})	6 M KOH	[31]
Ginkgo leaf	KOH	1538.7	345 (0.2 A g^{-1})	1 M KOH	[32]
Starch	$Mg(NO_3)_2$	2300	229 (1.0 A g^{-1})	6 M KOH	[33]
Tofu	$ZnCl_2$	1539	315 (0.5 A g^{-1})	6 M KOH	[34]
Rice straw	KOH	1122	337 (1.0 A g^{-1})	6 M KOH	[35]
Water chestnut	KOH	3401	346 (0.5 A g^{-1})	6 M KOH	[36]
Rubber wood	H_3PO_4	693	129 (1.0 mV s^{-1})	1 M H_2SO_4	[37]
Alginate	KOH	1811	188 (1.0 A g^{-1})	6 M KOH	[38]
Puffed rice	KOH	3326	334 (0.5 A g^{-1})	6 M KOH	[39]
Popcorn	KOH	3301	348 (0.2 A g^{-1})	6 M KOH	[40]
HPC-2	KOH	1657	349 (1.0 A g^{-1})	6 M KOH	This work

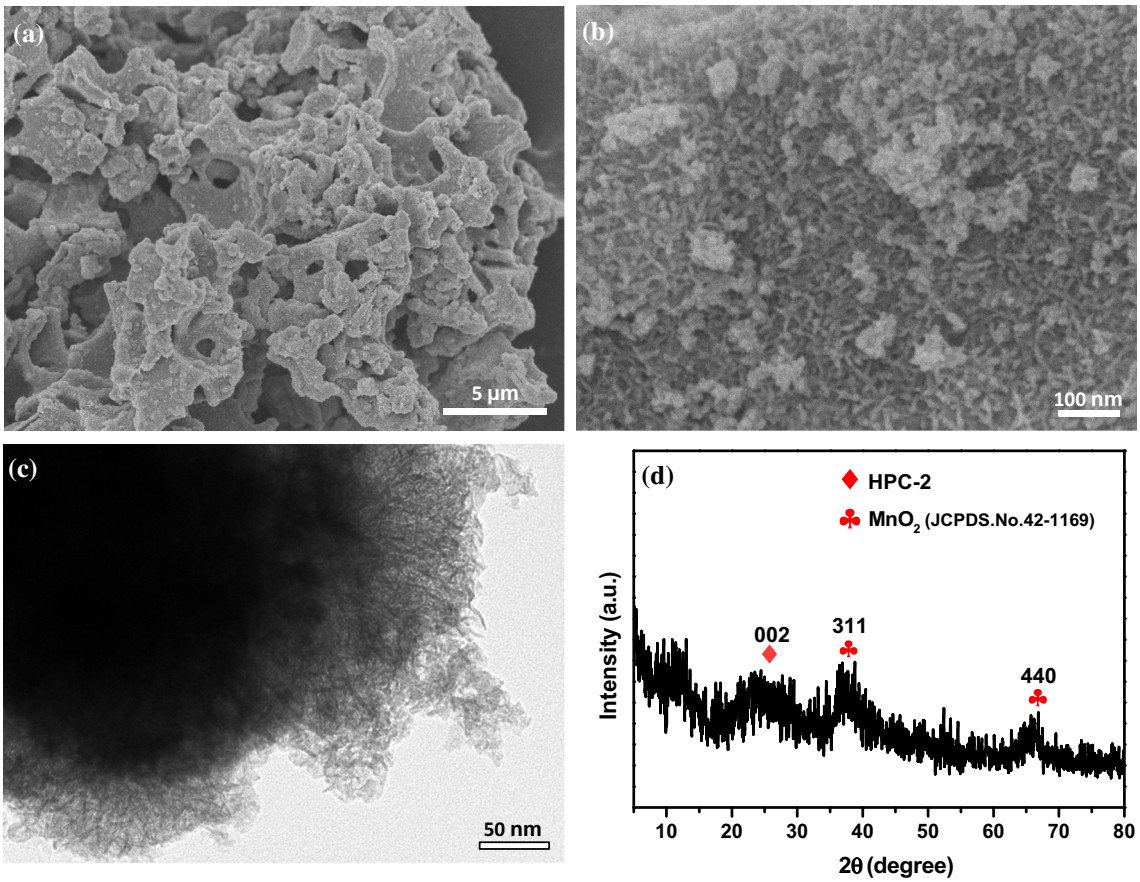

Figure 6 **a** SEM image of HPC-2/MnO_2. **b** High-resolution SEM images of HPC-2/MnO_2. **c** TEM image of HPC-2/MnO_2. **d** XRD patterns of the HPC-2/MnO_2 sample.

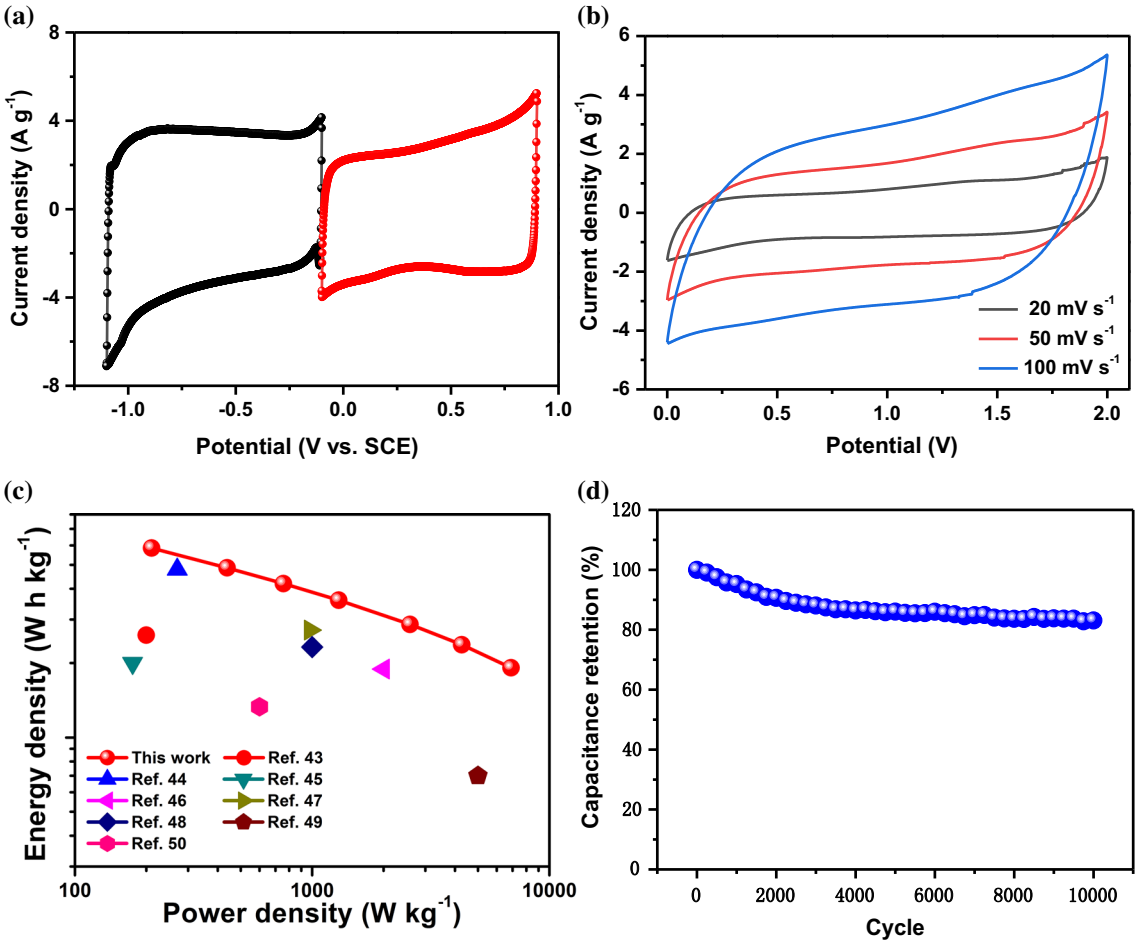

Figure 7 **a** CV curves of individual HPC-2 and HPC-2/MnO_2 composite electrodes in an aqueous solution Na_2SO_4 (1 mol L^{-1}) with the scan rate of 20 mV s^{-1}. **b** CV curves of assembled HPC-2//HPC-2/MnO_2 asymmetric supercapacitor with the scan rates from 20 to 100 mV s^{-1}. **c** Energy densities versus power densities and performance comparison of our asymmetric supercapacitor versus previously reported MnO_2-based asymmetric supercapacitor. **d** Cycling stability test of HPC-2//HPC-2/MnO_2 asymmetric supercapacitor measured at a current density of 200 mV s^{-1}.

rectangular-like shape with slight bumps, suggesting their specific capacity comes from double-layer capacitive and pseudocapacitance due to the existence of oxygen functional groups [25]. The HPC-2 sample has a larger CV curve area than the HPC-1 and HPC-3 samples, indicating a higher capacitance for HPC-2. The electrochemical characteristics of the obtained samples were further tested by galvanostatic charge/discharge measurement. As shown in Fig. 5b, the galvanostatic charge/discharge curve of the HPC-2 electrode at a current density of 1 A g^{-1} shows nearly linear and symmetric triangular shapes, indicating good capacitive property. Consistent with the CV results, the HPC-2 has a longer charge/discharge times than other materials. The specific capacity of HPC-2 from the discharge curve is calculated to be 349 F g^{-1} at a current density of 1 A g^{-1}, which is comparable to those of commercial activated carbon (YP-50), HPC-1, HPC-3 (Fig. 5c) and other reported biomass-based porous carbon materials (Table 1). Significantly, the HPC-2 electrode still shows a specific capacity of 247 F g^{-1} at a current density of 50 A g^{-1}, showing good rate characteristic due to its 3D interconnected honeycomb-like porous structure ensuring effective accessibility of electrolyte ions at high charge/discharge rates. Furthermore, the electrochemical stabilization of the HPC-2 electrode was performed at 200 mV s^{-1} for 10000 cycles. As shown in Fig. 5d, it can retain 98.6% of its initial capacity after 10000 cycles, showing outstanding electrochemical stabilization.

Recently, assembling asymmetric device is considered to be an effective way to improve the energy density of supercapacitor [9]. As a positive material, MnO_2 has attracted enormous attention because of its high theory capacity, wide voltage range and low cost [41]. Moreover, carbon materials can serve as sacrificial substrate to reduce potassium permanganate to form MnO_2 deposits, which can effectively improve the conductivity of MnO_2 [42]. SEM image of HPC-2/MnO_2 (Fig. 6a) still shows the 3D interconnected honeycomb-like porous structure. From high-resolution SEM image (Fig. 6b), it can be observed that rod-like MnO_2 grows uniformly on the HPC-2 surface. A high-resolution TEM image further confirms that the rod-like MnO_2 are closely growing on the carbon substrate surface with the lengths of 100–200 nm (Fig. 6c). Additionally, as shown in Fig. 6d, XRD pattern confirms the existence of MnO_2 with the diffraction peaks relevant to (311) and (440) planes, which can be attributed to birnessite-type MnO_2 (JCPDS 42-1169). The electrochemical characteristics of HPC-2/MnO_2 material were investigated in a three-electrode system in 1.0 M Na_2SO_4 aqueous electrolyte. The CV profiles of the HPC-2/MnO_2 material at different scan rates from 50 to 200 mV s^{-1} are shown in Fig. S3a. CV profile still keeps a nearly rectangular shape even at 200 mV s^{-1}, suggesting good rate performance. Additionally, the HPC-2/MnO_2 material shows a high specific capacity of 254 F g^{-1} at 2 mV s^{-1} (Fig. S3b),which is comparable with other carbon/MnO_2 composites (Table S1). Even at 200 mV s^{-1}, it shows a specific capacity of 201 F g^{-1}, meaning good rate performance.

An asymmetric supercapacitor (ASC) was assembled using the HPC-2/MnO_2 material as the positive electrode and the HPC-2 as the negative electrode in 1 M Na_2SO_4 aqueous electrolyte. CV tests were first utilized to estimate the electrochemical voltage window of individual electrode in a three-electrode system. The stable voltage windows are − 0.1 to 0.9 V for the HPC-2/MnO_2 electrode and − 1.1 to − 0.1 V for HPC-2 electrode in 1 M Na_2SO_4 solution (Fig. 7a). The stable working voltage range of the asymmetric supercapacitor could be extended up to 2.0 V, and no obvious distortion is observed even at a high scan rate of 100 mV s^{-1} (Fig. 7b). Benefitting from its high specific capacity and wide voltage window, the HPC-2//HPC-2/MnO_2 asymmetrical supercapacitor delivers a maximum energy density of 58.8 Wh kg^{-1} at a power density of 210.7 W kg^{-1}, which is much higher than the reported asymmetrical supercapacitors in aqueous electrolyte (Fig. 7c) [43–50]. Furthermore, the HPC-2//HPC-2/MnO_2 asymmetrical supercapacitor can maintain 83.1% of the initial capacity after 10000 cycles at 200 mV s^{-1}(Fig. 7d), demonstrating good electrochemical stability.

Conclusion

In this work, we develop a facile and sustainable method to synthesize 3D interconnected honeycomb-like porous carbon (HPC) derived from sunflowers stem. The optimized sample has large specific surface area with 3D interconnected porous structure and high oxygen content. Due to their synergistic effect, the HPC-2 material shows high specific capacitance, excellent rate capability and excellent cycling stability in 6 M KOH aqueous electrolyte. Moreover, the assembled HPC-2//HPC-2/MnO_2 asymmetric device shows a high energy density of 58.8 W h kg^{-1} and good electrochemical stabilization.

Acknowledgements

This work was supported by National Natural Science Foundation of China (51702043) and Fundamental Research Funds for the Central Universities (2572017BB18).

Compliance with ethical standards

Conflict of interest All authors listed have declared that they have no conflict of interest.

Electronic supplementary material: The online version of this article (https://doi.org/10.1007/s10853-018-03215-8) contains supplementary material, which is available to authorized users.

References

[1] Wang Q, Yan J, Fan ZJ (2016) Carbon materials for high volumetric performance supercapacitors: design, progress, challenges and opportunities. Energy Environ Sci 9(3):729–762

[2] Zang JF, Li XD (2011) In situ synthesis of ultrafine β-MnO_2/polypyrrole nanorod composites for high-performance supercapacitors. J Mater Chem 21:10965–10969

[3] Gao Z, Yang WL, Wang J, Song NN, Li XD (2015) Flexible all-solid-state hierarchical $NiCo_2O_4$/porous graphene paper asymmetric supercapacitors with an exceptional combination of electrochemical properties. Nano Energy 13:306–317

[4] Gao Z, Song NN, Li XD (2015) Microstructural design of hybrid CoO@NiO and graphene nano-architectures for flexible high performance supercapacitors. J Mater Chem A 3:14833–14844

[5] Qu QT, Shi Y, Li LL, Guo WL, Wu YP, Zhang HP, Guan SY, Holze R (2009) $V_2O_5{\cdot}0.6H_2O$ nanoribbons as cathode material for asymmetric supercapacitor in K_2SO_4 solution. Electrochem Commun 11(6):1325–1328

[6] Wu ZS, Parvez K, Feng XL, Mullen K (2013) Graphene-based in-plane micro-supercapacitors with high power and energy densities. Nat Commun 4:2487

[7] Jiang LL, Sheng LZ, Chen X, Wei T, Fan ZJ (2016) Construction of nitrogen-doped porous carbon buildings using interconnected ultra-small carbon nanosheets for ultra-high rate supercapacitors. J Mater Chem A 4(29):11388–11396

[8] Yan J, Fan ZJ, Sun W, Ning GQ, Wei T, Zhang Q, Zhang RF, Zhi LJ, Wei F (2012) Advanced asymmetric supercapacitors based on $Ni(OH)_2$/graphene and porous graphene electrodes with high energy density. Adv Funct Mater 22(12):2632–2641

[9] Wu XL, Jiang LL, Long CL, Wei T, Fan ZJ (2015) Dual support system ensuring porous Co–Al hydroxide nanosheets with ultrahigh rate performance and high energy density for supercapacitors. Adv Funct Mater 25(11):1648–1655

[10] Salunkhe RR, Tang J, Kamachi Y, Nakato T, Kim JH, Yamauchi Y (2015) Asymmetric supercapacitors using 3D nanoporous carbon and cobalt oxide electrodes synthesized from a single metal–organic framework. ACS Nano 9(6):6288–6296

[11] Zhang LL, Zhao XS (2009) Carbon-based materials as supercapacitor electrodes. Chem Soc Rev 38(9):2520–2531

[12] Qie L, Chen WM, Xu HH, Xiong XQ, Jiang Y, Zou F, Hu XL, Xin Y, Zhang ZL, Huang YH (2013) Synthesis of functionalized 3D hierarchical porous carbon for high-performance supercapacitors. Energy Environ Sci 6(8):2497–2504

[13] Wu XL, Jiang LL, Long CL, Fan ZJ (2015) From flour to honeycomb-like carbon foam: carbon makes room for high energy density supercapacitors. Nano Energy 13:527–536

[14] Zhang JL, Zhang WF, Zhang H, Pang J, Cao GP, Han MF, Yang YS (2017) A novel synthesis of hierarchical porous carbons from resol by potassium acetate activation for high performance supercapacitor electrodes. J Alloys Compd 712:76–81

[15] Gao Z, Zhang Y, Song NN, Li XD (2017) Biomass-derived renewable carbon materials for electrochemical energy storage. Mater Res Lett 5:69–88

[16] Gao Z, Song NN, Zhang YY, Schwab Y, He JJ, Li XD (2018) Carbon nanotubes derived from yeast-fermented wheat flour and their energy storage application. ACS Sustain Chem Eng 6:11386–11396

[17] Liu JJ, Deng YF, Li XH, Wang LF (2016) Promising nitrogen-rich porous carbons derived from one-step calcium chloride activation of biomass-based waste for high performance supercapacitors. ACS Sustain Chem Eng 4(1):177–187

[18] Zhang YY, Gao Z, Song NN, Li XD (2016) High-performance supercapacitors and batteries derived from activated banana-peel with porous structures. Electrochim Acta 222:1257–1266

[19] Gao Z, Zhang YY, Song NN, Li XD (2017) Towards flexible lithium–sulfur battery from natural cotton textile. Electrochim Acta 246:507–516

[20] Yao QF, Wang HW, Wang C, Jin CD, Sun QF (2018) One step construction of nitrogen-carbon derived from *Bradyrhizobium japonicum* for supercapacitor applications with a soybean leaf as a separator. ACS Sustain Chem Eng 6(4):4695–4704

[21] Wu XL, Wen T, Guo HL, Yang SB, Wang XK, Xu AW (2013) Biomass-derived sponge-like carbonaceous hydrogels and aerogels for supercapacitors. ACS Nano 7(4):3589–3597

[22] Ma GF, Yang Q, Sun KJ, Peng H, Ran FT, Zhao XL, Lei ZQ (2015) Nitrogen-doped porous carbon derived from biomass waste for high-performance supercapacitor. Bioresour Technol 197:137–142

[23] Zhao KM, Liu SQ, Ye GY, Gan QM, Zhou Z, He Z (2018) High-yield bottom-up synthesis of 2D metal–organic frameworks and their derived ultrathin carbon nanosheets for energy storage. J Mater Chem A 6(5):2166–2175

[24] Hu X, Xu XH, Zhong RQ, Shang LJ, Ma HT, Wu XL, Jia PY (2018) Facile synthesis of microporous carbons with three-dimensional honeycomb-like porous structure for high performance supercapacitors. J Electroanal Chem 823:54–60

[25] Ding B, Guo D, Wang YH, Wu XL, Fan ZJ (2018) Functionalized graphene nanosheets decorated on carbon nanotubes networks for high performance supercapacitors. J Power Sources 398:113–119

[26] Lee SW, Yabuuchi N, Gallant BM, Chen S, Kim BS, Hammond PT, Shao-Horn Y (2010) High-power lithium batteries from functionalized carbon-nanotube electrodes. Nat Nanotechnol 5(7):531–537

[27] Zhang WL, Lin HB, Lin ZQ, Yin J, Lu HY, Liu DC, Zhao MZ (2015) 3D hierarchical porous carbon for supercapacitors prepared from lignin through a facile template-free method. ChemSusChem 8(12):2114–2122

[28] Li Z, Zhang L, Amirkhiz BS, Tan XH, Xu ZW, Wang HL, Olsen BC, Holt CMB, Mitlin D (2012) Carbonized chicken eggshell membranes with 3D architectures as high-performance electrode materials for supercapacitors. Adv Energy Mater 2(4):431–437

[29] Sun L, Tian CG, Li MT, Meng XY, Wang L, Wang RH, Yin J, Fu HG (2013) From coconut shell to porous graphene-like nanosheets for high-power supercapacitors. J Mater Chem A 1(21):6462–6470

[30] Ganesan A, Mukherjee R, Raj J, Shaijumon MM (2014) Nanoporous rice husk derived carbon for gas storage and high performance electrochemical energy storage. J Porous Mater 21(5):839–847

[31] Yu S, Zhu XQ, Lou GB, Wu YT, Xu KT, Zhang Y, Zhang LM, Zhu EH, Chen H, Shen ZH, Bao BF, Fu SY (2018) Sustainable hierarchical porous biomass carbons enriched with pyridinic and pyrrolic nitrogen for asymmetric supercapacitor. Mater Des 149:184–193

[32] Wang J, Zhang PX, Liu L, Zhang Y, Yang JF, Zeng ZL, Deng SG (2018) Controllable synthesis of bifunctional porous carbon for efficient gas-mixture separation and high-performance supercapacitor. Chem Eng J 348:57–66

[33] Cao JH, Zhu CY, Aoki Y, Habazaki H (2018) Starch-derived hierarchical porous carbon with controlled porosity for high performance supercapacitors. ACS Sustain Chem Eng 6(6):7292–7303

[34] Yao L, Yang JJ, Zhang PX, Deng LB (2018) In situ surface decoration of $Fe_3C/Fe_3O_4/C$ nanosheets: towards bifunctional activated carbons with supercapacitance and efficient dye adsorption. Bioresour Technol 256:208–215

[35] Liu SB, Zhao Y, Zhang BH, Xia H, Zhou JF, Xie WK, Li HJ (2018) Nano-micro carbon spheres anchored on porous carbon derived from dual-biomass as high rate performance supercapacitor electrodes. J Power Sources 381:116–126

[36] Wei HM, Chen J, Fu N, Chen HJ, Lin HL, Han S (2018) Biomass-derived nitrogen-doped porous carbon with superior capacitive performance and high CO_2 capture capacity. Electrochim Acta 266:161–169

[37] Thubsuang U, Laebang S, Manmuanpom N, Wongkasemjit S, Chaisuwan T (2017) Tuning pore characteristics of porous carbon monoliths prepared from rubber wood waste treated with H_3PO_4 or NaOH and their potential as supercapacitor electrode materials. J Mater Sci 52:6837–6855. https://doi.org/10.1007/s10853-017-0922-z

[38] Wang BB, Li DH, Tang MW, Ma HB, Gui YG, Tian X, Quan FY, Song XQ, Xia YZ (2018) Alginate-based hierarchical porous carbon aerogel for high-performance supercapacitors. J Alloys Compd 749:517–522

[39] Hou JH, Jiang K, Tahirc M, Wu X, Idreesc F, Shen M, Cao CB (2017) Tunable porous structure of carbon nanosheets derived from puffed rice for high energy density supercapacitors. J Power Sources 371:148–155

[40] Hou JH, Jiang K, Wei R, Tahir M, Wu XG, Shen M, Wang XZ, Cao CB (2017) Popcorn-derived porous carbon flakes with an ultrahigh specific surface area for superior performance supercapacitors. ACS Appl Mater Interfaces 9:30626–30634

[41] Tao XY, Du J, Sun Y, Zhou SL, Xia Y, Huang H, Gan YP, Zhang WK, Li XD (2013) Exploring the energy storage mechanism of high performance MnO_2 electrochemical capacitor electrodes: an in situ atomic force microscopy study in aqueous electrolyte. Adv Funct Mater 23:4745–4751

[42] Li YH, Fu HY, Zhang YF, Wang ZY, Li XD (2014) Kirkendall effect induced one-step fabrication of tubular Ag/MnO_x nanocomposites for supercapacitor application. J Phys Chem C 118:6604–6611

[43] Li YJ, Chen CJ, Gao TT, Zhang DM, Huang XM, Pan Y, Ye K, Cheng K, Cao DX, Wang GL (2016) Synthesis of hierarchically porous sandwich-like carbon materials for high-performance supercapacitors. Chem Eur J 22(47):16861–16869

[44] Wang Y, Lai WH, Wang N, Jiang Z, Wang XY, Zou PC, Lin ZY, Fan HJ, Kang FY, Wong CP, Yang C (2017) A reduced graphene oxide/mixed-valence manganese oxide composite electrode for tailorable and surface mountable supercapacitors with high capacitance and super-long life. Energy Environ Sci 10(4):941–949

[45] Cakici M, Reddy KR, Alonso-Marroquin F (2017) Advanced electrochemical energy storage supercapacitors based on the flexible carbon fiber fabric-coated with uniform coral-like MnO_2 structured electrodes. Chem Eng J 309:151–158

[46] Zhao YF, Ran W, He J, Huang YZ, Liu ZF, Liu W, Tang YF, Zhang L, Gao DW, Gao FM (2015) High-performance asymmetric supercapacitors based on multilayer MnO_2/-graphene oxide nanoflakes and hierarchical porous carbon with enhanced cycling stability. Small 11(11):1310–1319

[47] Yu N, Yin H, Zhang W, Liu Y, Tang ZY, Zhu MQ (2016) High-performance fiber-shaped all-solid-state asymmetric supercapacitors based on ultrathin MnO_2 nanosheet/carbon fiber cathodes for wearable electronics. Adv Energy Mater 6(2):1501458

[48] Gao HC, Xiao F, Ching CB, Duan HW (2012) High-performance asymmetric supercapacitor based on graphene hydrogel and nanostructured MnO_2. ACS Appl Mater 4(5):2801–2810

[49] Wu ZS, Ren WC, Wang DW, Li F, Liu BL, Cheng HM (2010) High-energy MnO_2 nanowire/graphene and graphene asymmetric electrochemical capacitors. ACS Nano 4(10):5835–5842

[50] Li L, Hu ZA, An N, Yang YY, Li ZM, Wu HY (2014) Facile synthesis of MnO_2/CNTs composite for supercapacitor electrodes with long cycle stability. J Phys Chem C 118(40):22865–22872